ACADEMIC PRESS

Available online at www.sciencedirect.com

SCIENCE DIRECT®

Journal of Magnetic Resonance 161 (2003) 222–233

JMR Journal of Magnetic Resonance

www.elsevier.com/locate/jmr

A method for rapid characterization of diffusion

Y.-Q. Song,* M.D. Hürlimann, and C. Flaum

Schlumberger-Doll Research, 36 Old Quarry Road, Ridgefield, CT 06877, USA

Received 25 October 2002; revised 31 December 2002

Abstract

This paper describes a method to determine molecular displacements as a function of time in just two scans: one reference scan using the Carr–Purcell–Meiboom–Gill (CPMG) sequence, a second scan using a modified CPMG sequence (KCPMG). Measurements on free diffusion in bulk fluids, and on restricted diffusion in porous rock samples are reported. This technique can also be used for rapid measurement of flow and chemical exchange.

Keywords: Diffusion; CPMG; Porous media

1. Introduction

Measurement of the diffusion constant can assist the characterization of molecules and fluids. The time-dependent diffusion constant can be used to characterize pore geometry, such as surface-to-volume ratio and tortuosity [1,2] and it has been used to study rocks by applying pulsed or static field gradients [3–5]. In these NMR experiments using spin echo and stimulated echo, for example, one diffusion time (Δ) will be preset in the pulse sequence to determine the molecular displacement over Δ, thus obtaining $D(\Delta)$. Then, a series of measurements are made with different Δs to acquire the full curve of the time-dependent diffusion constant. Measurements of diffusion using Carr–Purcell–Meiboom–Gill (CPMG) sequence alone [6,7] would result in Δ comparable to the time between the $\pi/2$ and the first π pulses [8–11].

This paper describes an alternative experimental scheme to determine the molecular displacement at many values of Δ in one or a few scans of a modified CPMG sequence, called KCPMG. The key to our modification of CPMG is the creation of a spatially modulated magnetization at the beginning portion of the sequence and then to use the CPMG π pulse train to monitor the evolution of the modulation. In contrast, the initial magnetization in CPMG is uniform. In the case of spatial diffusion, the amplitude of the magnetization modulation is governed by the diffusion dynamics. We demonstrate that our scheme measures directly the time dependent diffusion. We present the concept of KCPMG and several implementations with different spatial modulations of the magnetization.

The KCPMG concept is closely related to the early work of Packer [12] in an effort to monitor the flow of fluids, using a rather weak field gradient. We will show that the presence of a strong magnetic field gradient changes the behavior of the echo formation that includes contributions from many coherence pathways. In fact, such large field inhomogeneities lead to a consistent echo shape that facilitates the determination of diffusion properties.

2. KCPMG methodology

2.1. CPMG and coherence pathways

The conventional CPMG sequence begins with a $\pi/2$ radio-frequency (RF) pulse, a waiting period T_{cp}, followed by a train of π pulses separated in time by $2T_{cp}$. This is commonly described by

$$\frac{\pi}{2} - T_{cp} - \left[\pi - 2T_{cp}\right]_N. \tag{1}$$

* Corresponding author. Fax: 1-2034383819.
E-mail address: ysong@slb.com (Y.-Q. Song).

1090-7807/03/$ - see front matter © 2003 Elsevier Science (USA). All rights reserved.
doi:10.1016/S1090-7807(03)00009-0

The brackets denote the repeating unit and N is the total number of echoes. The acquisition of echoes is made between the adjacent pairs of π pulses. We consider the application of a constant field gradient (G) during the CPMG and all other pulse sequences discussed in this paper. It has been shown recently that in a strong field gradient, the delay after the initial $\pi/2$ pulse (of length $t_{\pi/2}$) should be reduced to $T'_{cp} = T_{cp} - 2t_{\pi/2}/\pi$ in order to compensate for the precession during the $\pi/2$ pulse [13],

$$\frac{\pi}{2} - T'_{cp} - \left[\pi - 2T_{cp}\right]_n. \tag{2}$$

It is beneficial to discuss the CPMG-related sequences in terms of coherence pathways [14], in particular, for experiments in strong field gradients when the signal bandwidth is limited by the power of RF pulses. In this case, the nutation angle and the orientation of the rotation axis of a pulse depend on the offset between the frequency of the spin's Larmor precession and the RF irradiation [15,16]. As a result, many trajectories of the magnetization evolution contribute to the echo signals [17–21]. Goelman and Prammer [17] have partitioned these coherence pathways into direct echo and indirect echoes using a subset of the pathways that are most important. Hürlimann [21] has recently presented a thorough analysis of all coherence pathways and the diffusion effects. We will briefly introduce the basic notation of coherence pathways for CPMG here and will further discuss the coherence pathways of KCPMG in Appendix A.

We follow the notations used in [21] to mark the magnetization states by q which can be 0, +1, or −1, (or 0, +, and −), corresponding to z-, clockwise or counterclockwise precessing magnetizations. The RF pulses rotate the magnetization vector and thus change q. A coherence pathway is characterized by a series of numbers, $Q_N \equiv (q_0, q_1, \ldots, q_N)$, where q_0 is the coherence before the first π pulse and N is the echo number. We will follow [11] to highlight two types of coherences, the direct spin echo (SE) and the stimulated echo (STE). The direct spin echo is characterized by a series of qs that alternate between + and −. The stimulated echoes, on the other hand, have a few qs being zero corresponding to magnetization along the z-axis. For the CPMG sequence, the echoes for these two types of pathways form midway between two adjacent π pulses. However, in KCPMG, the echoes form at different times.

The contribution of a coherence pathway to the Nth echo can be written as a product of two factors, $M_{Q_N} = A_Q \cdot S_Q$. A_Q is a factor determined by the RF pulses. For a given coherence pathway, it can be identical for KCPMG and CPMG. S_Q describes the decay factor due to diffusion for a coherence pathway and is independent of the frequency offset. S_Q for KCPMG is different from that for CPMG. As a result, KCPMG is sensitive to diffusion over long diffusion times.

2.2. KCPMG pulse sequence

The concept of KCPMG can be implemented in several different ways. The simplest form consists of a CPMG sequence with an extra delay T_m inserted between the first $\pi/2$ and π pulses:

$$\frac{\pi}{2} - T_m - T'_{cp} - \left[\pi - 2T_{cp}\right]_n. \tag{3}$$

T_m can be positive or negative and $|T_m| = \delta < T_{cp}$. For positive T_m, the duration between the $\pi/2$ and the first π pulse is $T'_{cp} + \delta$, and for negative T_m, it is $T'_{cp} - \delta$. CPMG sequence corresponds to $T_m = 0$. We assume here that a constant magnetic field gradient G is applied. The same RF sequence was considered by Packer [12] with a weak gradient, i.e., $\gamma G L t_\pi < 1$, where L is the sample length along the gradient direction. In this case, the RF pulses can excite the entire sample and the nutation angle of the π pulse is close to 180° for the entire sample. Thus, the magnetization is being well refocused by the π pulses for the early echoes and these echo signals are dominated by one main coherence pathway (direct echo). This can also be done by including gradient pulses between the RF pulses, for example. However, for the later echoes, effects from minute errors of the pulses and RF field inhomogeneity will become significant so that other coherence pathways may not be neglected. As a result, the echo amplitude and shape will change and likely oscillate. In this work, we consider the presence of a strong field gradient, $\gamma G L t_\pi > 1$. This changes the spin dynamics by allowing many more coherence pathways to contribute appreciably. We will show that this condition produces consistent echo shapes which is helpful for a simple interpretation of the echo signal.

Phase cycling was used to select only coherence pathways that produce transverse magnetization after the first $\pi/2$ pulse. For the pulse sequences in Eqs. (1) and (3), the phase of the first $\pi/2$ pulse was alternated between 0° and 180°. The π pulses were at 90° phase. The data from the two phase settings are subtracted from each other. In addition, a four-phase CYCLOP scheme can be applied to further remove systematic errors. We will first examine this simple implementation of KCPMG in some details before discussing other implementations.

A similar RF sequence coupled with pulsed field gradients has also been reported [22] with a goal of producing multiple echoes and accelerating imaging experiments.

2.3. Echo shapes

The peaks of KCPMG echoes form at times shifted by $+\delta$ (late echoes) or $-\delta$ (early echoes) relative to the corresponding positions of the CPMG echoes ($\delta = |T_m|$). The shapes of several echoes obtained with the CPMG

Eq. (2) and KCPMG Eq. (3) sequences are compared in Fig. 1. Panels (a) and (b) show the KCPMG echoes with $T_m = -0.9$ and +0.9 ms, and $\delta = 0.9$ ms. Panel (c) shows the shape of the CPMG echoes from the first Hahn echo to the later ones with the asymptotic echo shape in a constant field gradient. It is typical for the CPMG asymptotic echo to develop small negative amplitudes at the edges of the echo [21]. The first echo occurs at a time $T_{cp} - \delta$ after the π pulse and has the shape of the Hahn echo since the direct echo is the only possible coherence pathway. The second detection period displayed below shows two echoes appearing at times $T_{cp} + \delta$ and $T_{cp} - \delta$ after the second π pulse. The two echoes have different shapes because they are formed by different coherence pathways, with the early one being a stimulated echo ($Q = +0-$) and the late one being a direct echo ($Q = - + -$). For echoes in the later periods after many π pulses, both direct and stimulated echo-like coherence pathways contribute giving rise to their unique, asymptotic shapes. The echoes at times $T_{cp} + T_m$ are contributed by the coherence pathways starting with $q_0 = -1$, while the echoes at times $T_{cp} - T_m$ are contributed by those starting with $q_0 = +1$. For CPMG, i.e., $T_m = 0$, the signals from these different coherence pathways overlap midway between two π pulses. The non-zero T_m in KCPMG allows the separate observation of these different coherence pathways directly. For the second echo, this technique has also been used by Bãlibanu et al. [20] to separate the two contributions.

The KCPMG sequence [Eq. (3)] with positive T_m produces a similar echo evolution as discussed above for negative T_m, but with the early and late echoes reversed, Fig. 1b.

The addition of the data from sequences with T_m and $-T_m$ (Fig. 1d) cancels much of the secondary features of the echoes and makes the shapes of the KCPMG echo much more similar to those of the CPMG echoes. In this symmetrized form, the same coherence pathways contribute to both the early and late KCPMG echoes and these pathways are identical to those of the corresponding CPMG echoes. Thus, this is the preferred scheme to execute the KCPMG.

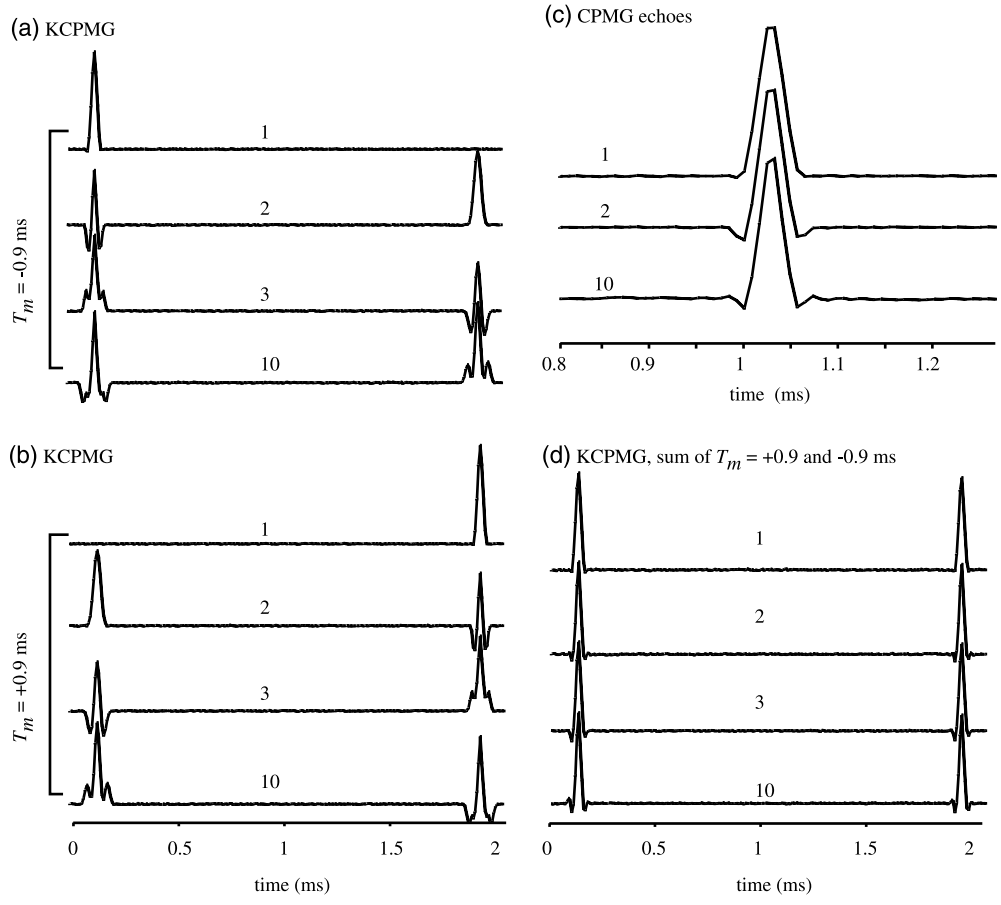

Fig. 1. CPMG and KCPMG echoes vs the detection time starting after the π pulse, for tap water at $\delta = 0.9$ ms. $T_{cp} = 1.1$ ms. The data for each signal is labelled by the echo number. The sample shape is a cylinder of 2 cm diameter and 4 cm length. The magnetic field is 410 G corresponding to the proton Larmor frequency of 1.7 MHz. The applied magnetic field gradient is 13.2 G/cm and the duration of the $\pi/2$ pulse is 12 μs. Only a slice of about 5 mm in the center of the sample was excited by the RF pulses. Experiments were performed using an Apollo spectrometer from Tecmag.

2.4. Decay due to diffusion

The decay of signal of fluids during the CPMG in the presence of field gradients is dominated by two sources. The first is the intrinsic bulk spin–spin relaxation and that due to interactions with the surfaces. The second source is the Brownian motion of fluid molecules in the presence of inhomogeneous magnetic fields. At the middle of the adjacent π pulses, the accumulated phase from Larmor precession is zero on average, however, the phase dispersion due to diffusion renders some of the spins out of phase leading to signal decay. Since the average phase is zero, the final effect of diffusion is an attenuation of the signal.

Although the KCPMG sequence [Eq. (3)] may appear almost identical to CPMG, the spin dynamics however retains an additional element of evolution. It is instructive to view the KCPMG pulse sequence in two segments. The first segment includes the first $\pi/2$ pulse and the following time period T_m. The second segment starts at the end of T_m and extends to the rest of the sequence. This second segment is identical to the CPMG sequence since the magnetization starts in the transverse plane. Our understanding of the CPMG sequence states that at any time in the middle of the two adjacent π pulses the average phase is zero and the effect of diffusion is just an attenuation factor. This attenuation factor can be obtained from a CPMG measurement with the same T_{cp}.

The presence of the first segment produces a spatially modulated magnetization, at time T_m, with a modulation wavelength:

$$\lambda = 2\pi/(\gamma G\delta), \tag{4}$$

where γ is the gyromagnetic ratio of the detected nuclei, G is the magnetic field gradient. One may also define a wave vector

$$K \equiv 2\pi/\lambda = \gamma G\delta, \tag{5}$$

as in magnetic resonance imaging [23,24]. These K-states of magnetization modulation, hence the name "KCPMG," are the eigenstates of diffusion in bulk fluids and the amplitude of the K-states decays exponentially [3,25] with the decay rate:

$$R(K) = DK^2, \tag{6}$$

where D is the diffusion constant, defined from the mean square displacement ($\langle r^2\rangle$), $D = \langle r^2\rangle/6\Delta$ where Δ is the observation time. In bulk fluids, D is a constant. For diffusion in porous media, the above sinusoidal modulation is no longer the eigenstate of the diffusion dynamics resulting in that D can depend on Δ.

Thus, the effect of the first part of KCPMG is to prepare a spatially modulated magnetization state and the second part monitors the evolution of this K-state. The KCPMG echoes appearing off center should be viewed as the time-domain signal of the K-states with the time origin at the CPMG echo position. On the other hand for the case of the CPMG, the initial state is a spatially uniform magnetization. Thus, one would expect that the signals from KCPMG sequence will have an additional decay $\exp[-R(K)t]$:

$$S(K,t) \approx S(0,t)\cdot \mathrm{e}^{-DK^2t}, \tag{7}$$

t is echo time, $t = 2NT_{cp}$ and N is the echo number. The signal $S(0,t)$ is in fact the CPMG data since it corresponds to $T_m = 0$ and thus $K = 0$. In the later sections, we will present experimental results confirming Eq. (7). Detailed spin dynamics calculations including the effects of finite pulse length and gross field inhomogeneity have confirmed that Eq. (7) is a good ansatz. We will outline the more detailed theory for KCPMG in Appendix A.

2.5. Correction for spin–spin relaxation

For samples with short relaxation times, a correction term has to be added to Eq. (7). Since the KCPMG echoes appear at different times than the CPMG echoes, transverse relaxation affects KCPMG and CPMG differently if relaxation is important during the time δ. For example, with $T_m = +\delta$, the two Nth echoes of the KCPMG sequence appear at $2NT_{cp}$ and $2NT_{cp} + 2\delta$ after the initial $\pi/2$ pulse. Thus, a correction term to compensate for such different echo times can be included in Eq. (7):

$$S(K,t) \approx S(0,t)\cdot \frac{1}{4}(2 + \mathrm{e}^{-2\delta/T_2} + \mathrm{e}^{2\delta/T_2})\cdot \mathrm{e}^{-DK^2t}, \tag{8}$$

where T_2 is the spin–spin relaxation of the fluid, including surface contributions. We shall denote A for the relaxation factor: $A \equiv \frac{1}{4}(2 + \mathrm{e}^{-2\delta/T_2} + \mathrm{e}^{2\delta/T_2})$. For $\delta \ll T_2$ as is the case for our experiments shown later, A can be well approximated by 1.

2.6. Alternative KCPMG sequences

There are various means to create the initial spatial modulation of the magnetization essential for the KCPMG concept. In a second implementation a z-magnetization modulation is created and refocused with the following sequence

$$\frac{\pi}{2} - \delta - \frac{\pi}{2} - T_d - \frac{\pi}{2} - T_{cp} - \left[\pi - 2T_{cp}\right]_n. \tag{9}$$

The phases used for the first three pulses are: (0° 180°), (0° 0° 180°180°), and 0°. The phase of all π pulses is 90°. The receiver phases are: 0° 180° 180° 0°. The first $\pi/2$ pulse rotates the magnetization to the transverse plane for precession under the field gradient. The second $\pi/2$ pulse stores the magnetization modulation along the longitudinal direction. The wave length of the modulation is again given by Eq. (4). The transverse magnetization at the end of the second $\pi/2$ pulse can be removed

by proper phase cycling or inclusion of a crusher gradient. The rest of the sequence is identical to the CPMG. The first three pulses form the usual stimulated echo sequence and T_d is the initial diffusion time. The first echo after the third $\pi/2$ pulse is a stimulated echo. For the Nth echo, the diffusion time is $\Delta = T_d + 2NT_{cp}$.

More complex modulation scheme can be implemented in the initial part of the sequence. For example, if an initial modulation consists of a superposition of uniform magnetization with a modulated magnetization, then one scan of the KCPMG sequence can obtain decays for multiple values of K.

In an example of such complex modulation, the CPMG sequence is preceded by three pulses:

$$\frac{\pi}{2} - \delta/2 - \theta_1 - \delta/2 - \theta_2 - T_{cp} - \left[\pi - 2T_{cp}\right]_n. \qquad (10)$$

θ_1 and θ_2 are RF pulses with tipping angles θ_1 and θ_2. The first two pulses create magnetization with a modulation characterized by $K = \pm K_0, \pm K_0/2$, and 0, where $K_0 = \gamma G\delta$. The tipping angle θ_2 of the third pulse as well as the phase cycling for the first three pulses control the weight of the different modulations. Five echoes will be observed between the adjacent π pulses. Echoes for different modulations are shifted by a different time, $\pm|K|/(\gamma G)$, from the nominal CPMG echo position. Thus in a single scan, three decays for $|K| = 0, K_0/2, K_0$ can be obtained simultaneously.

3. Experimental verifications

3.1. Bulk fluids

The KCPMG technique was tested on a sample of tap water using a Bruker Avance NMR spectrometer at a proton Larmor frequency of 85 MHz. The pulse sequence in Eq. (9) was used with an additional crusher gradient during T_d to remove the transverse components. A z-gradient of 10 G/cm was applied during the encoding and CPMG. A y-gradient of 5 G/cm was used during the crusher period (T_d). T_{cp} was 2 ms and T_m varied from 0.5 to 1.9 ms. In Fig. 2, the decay for all values of T_m is approximately exponential and the decay rate increases as T_m increases. The initial KCPMG signals are about half of the CPMG signal because only one KCPMG echo was detected. The signals of early echoes showed additional oscillations due to the evolution in the echo shape. The decay rate for each value of T_m was calculated from the data and plotted in the inset of Fig. 2 as a function of T_m^2. The linearity and values of the additional decay rate is consistent with Eq. (6) for the decay of K-modes. Therefore, these data are consistent with Eq. (7).

Similar experiments were performed on an oil sample which is often used as a viscosity standard (S6, Cannon Instrument Company, P.O. Box 16, State College, PA). The CPMG and KCPMG data presented in Fig. 3 show a small additional decay in KCPMG compared to CPMG, in contrast to the much larger additional decay observed for water in Fig. 2. This is an indication of the much smaller diffusion constant of S6 oil, consistent

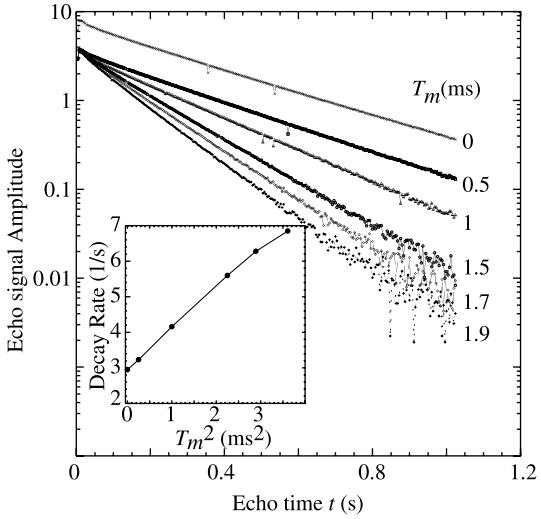

Fig. 2. KCPMG measurements for water at several T_ms. The CPMG data corresponds to $T_m = 0$. The pulse sequence used was Eq. (9), $T_{cp} = 2$ ms and $T_d = 5.3$ ms. The magnetic field gradient applied during the encoding and CPMG is 10 G/cm along z. A crusher gradient of 5 G/cm (y) was applied during T_d. Signals were acquired at the peak of the early echoes. *Inset*: Decay rate R for KCPMG as a function of T_m^2. The linear dependence of R with T_m^2 is consistent with Eq. (6) and the extracted diffusion constant for water is 1.5×10^{-5} cm^2/s at 14 °C. The apparent glitches in the data were caused by intermittent receiver problems.

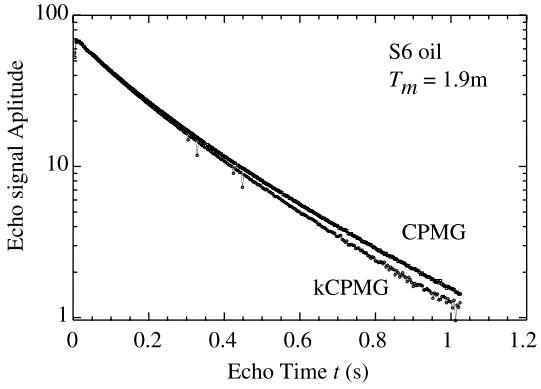

Fig. 3. Comparison of KCPMG measurement for S6 oil at T_m of 1.9 ms with CPMG data. In both cases, $T_{cp} = 2$ ms and the magnetic field gradient used was 10 G/cm. From the extra decay of the KCPMG data compared to the CPMG, the diffusion constant of the S6 oil was determined to be 0.82×10^{-6} cm^2/s at 14 °C. The apparent glitches in the KCPMG data around 0.4 s were caused by receiver problems. The experiments were performed on a Bruker Avance spectrometer at 85 MHz. The KCPMG echo signal is detected at the early echo and the amplitude is scaled up by factor of 2 in order to facilitate comparison with CPMG data in the figure.

with independent measurements using the pulsed field gradient method [26].

3.2. Restricted diffusion

It is well-known that diffusion in porous media is restricted in the sense that the mean square displacement of molecules is less than that for the bulk fluid [1,27]. It is often expressed as a reduced diffusion constant that is dependent on the diffusion time. For example, Mitra et al. [2] showed that such time-dependent diffusion constant can be used as a measure of the surface-to-volume ratio of materials. In addition, at long time when the molecular diffusion distance exceeds the characteristic length scale, such as the pore size, the diffusion constant reaches an asymptotic value that is a function of the connectivity of the pore system, $D(\infty) = D_0/F\phi$, where ϕ is the porosity of the sample. F is the formation factor, an important characteristic of porous materials.

Here, we utilize the effect of restricted diffusion and the resulting time dependent displacement as a stringent experimental test of the concept of KCPMG. In particular, we will show that the diffusion time in a KCPMG experiment is the time between the initial modulation and the detection of the Nth echo, i.e., $\Delta \approx 2NT_{cp}$.

For bulk fluids, since D is a constant independent of Δ, it is difficult to prove that our measurements presented in the previous section are a measure of the true long-time displacements. In addition, while our analytical theory of the KCPMG sequence can be used to calculate in detail the effects of bulk diffusion, it is difficult to evaluate in detail the effects of restricted diffusion. Each coherence pathway will have to be individually analyzed for restricted diffusion as it was reported for the direct echo pathway [8].

3.3. Brine saturated rocks

The KCPMG experiments on rocks were performed at low magnetic field of about 410 G in order to reduce the effects of internal field inhomogeneity due to susceptibility contrast. The NMR spectrometer operated at a Larmor frequency of 1.7 MHz. Rock samples were cylinders of 20 mm diameter and 38 mm length. The samples were placed in the fringe field of a superconducting magnet where the constant field gradient applied across the sample was 13.2 G/cm. The samples were saturated with brine similar to the borehole salinity. The $\pi/2$ and π pulses are 12 and 24 μs long, respectively, exciting an approximately 5 mm slice of the sample perpendicular to the direction of the field gradient.

Fig. 4a shows the data of KCPMG and CPMG on a sample of brine saturated Berea sandstone. The decays are approximately exponential, although there is a slight curvature at short times. This is consistent with a relatively narrow distribution of pore sizes in this type of rock. The mean square displacement of water due to diffusion versus time, obtained by $\log[S(K,t)/S(0,t)A]/K^2$, is shown in Fig. 4b and compared with that of bulk water. It is clear that the displacement in the rock is reduced compared to that in bulk water, a result consistent with the concept of restricted diffusion. The line in the figure is a fit to the short time data of Berea. It highlights the deviations of the Berea data at long time, indicating that the diffusion is being further slowed down at later times and that the diffusion cannot be described by a time-independent diffusion coefficient. Fig. 5 shows the time-dependent diffusion constant obtained from the KCPMG data as a function of time. Since $D(t)$ is expected to change with time only smoothly, each point in Fig. 5 represents an average of five original data points. The reduction of $D(t)$ at long time is clear. In addition, $D(t)$ by KCPMG is in

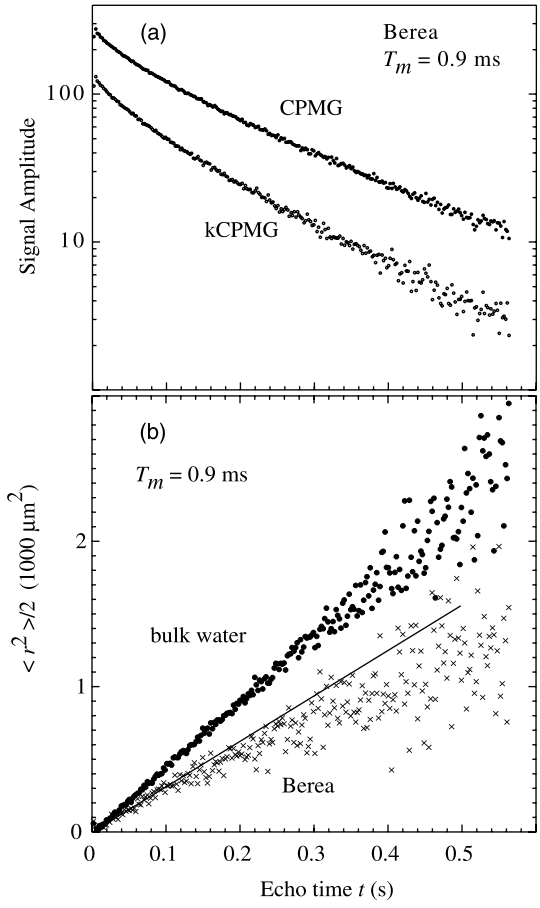

Fig. 4. (a) KCPMG measurements for the Berea sample with $T_m = 0.9$ ms, compared with the CPMG data. $T_{cp} = 1.1$ ms. The magnetic field gradient is 13.2 G/cm. (b) A plot of the mean square displacement extracted from the KCPMG and CPMG measurements for water in the Berea sample (crosses) versus time. The data for bulk water (circles) were obtained under identical condition and are shown as a comparison. Clearly, the displacement of water in the Berea sample is reduced compared to that in bulk. The line is a fit to the displacement for Berea at early times showing that diffusion at long time is further reduced.

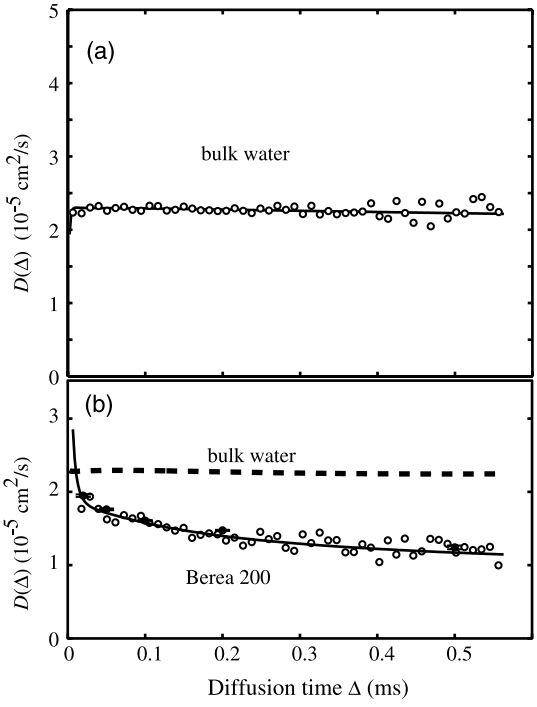

Fig. 5. The time-dependent diffusion constant $D(\Delta)$ for: (a) the bulk water sample and (b) the Berea sample obtained from the KCPMG and CPMG data as a function of echo time. For KCPMG, the diffusion time Δ is $2NT_{cp}$. In (b), the filled circles show $D(\Delta)$ obtained using conventional stimulated echo technique on the same sample. The results are consistent with the KCPMG results. The line is obtained by Eq. (7) using the multi-exponential fits to the KCPMG and CPMG decay data. The corresponding measurement on bulk water is shown as the dotted line for comparison. The gradual reduction of $D(\Delta)$ at long time is clear.

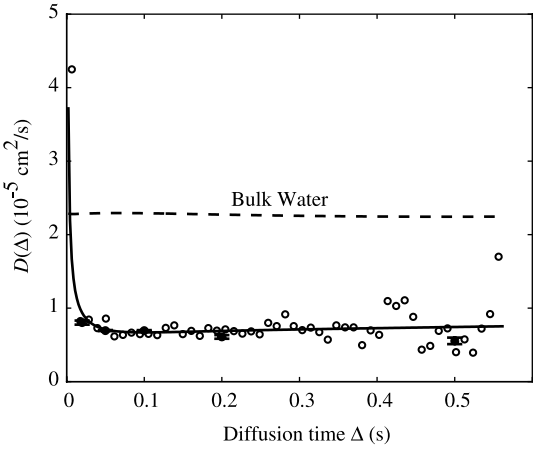

Fig. 6. The time-dependent diffusion constant $D(\Delta)$ for water saturated carbonate rock obtained from the KCPMG and CPMG data as a function of echo time (open circles). For KCPMG, the diffusion time Δ is $2NT_{cp}$. Each data point represents the average of five original data points at nearby echo times. The noise is quite significant for echo time longer than 0.3 s. $D(\Delta)$ obtained using stimulated echo technique on the same sample is shown as the black circles. The observed saturation of $D(\Delta)$ is consistent with the long time limit obtained independently from the measured formation factor and porosity.

complete agreement with the data obtained with stimulated echo experiments in a constant gradient [5].

At long diffusion time t when the molecules have diffused a distance larger than the pore spacing, $D(t)$ approaches a constant, $D(\infty) = D_0/F\phi$. For samples with large pores, such as Berea sandstone, this limit can be reached only at long time and is difficult to measure directly due to short spin relaxation time. For example, it takes 2 s for water to diffuse 100 μm, which is much longer than the T_1 or T_2 relaxation times in Berea. However, in fine grained rocks such as mudstones, this limit can be reached within a time shorter than the relaxation time [28]. Fig. 6 shows an example where the long time limit is observed. The sample is a carbonate rock with pore sizes on the length scale of a few microns. The two data sets shown in Fig. 6 agree for times larger than 50 ms and $D(t)$ saturates at about 0.7×10^{-5} cm^2/s, consistent with the long time limit.

4. Presence of grossly inhomogeneous fields

The experimental results shown in the sections above have demonstrated that Eq. (7) is a good ansatz for our measurements and that it allows the extraction of the diffusion coefficient at multiple diffusion times in a single scan.

In grossly inhomogeneous fields, the KCPMG signal contains contributions from many different coherence pathways. It would be natural to expect that contributions from some of the coherence pathways do not follow the simple relationship of Eq. (7). In fact, Eq. (7) is only a valid approximation for some of the coherence pathways. For example, let us consider the ninth echo, i.e., $N = 9$, and one such coherence pathway is $Q = (+++++---\!-)$. This is equivalent to a spin-echo with a an effective pulse spacing between the $\pi/2$ and π pulse of $9T_{cp}$. Thus, this coherence pathway contributes to the KCPMG signal (summing contributions from positive and negative values of T_m) as

$$\begin{aligned} S_Q &= \mathrm{e}^{-(2/3)D(\gamma G)^2(9T_{cp}+\delta)^3} + \mathrm{e}^{-(2/3)D(\gamma G)^2(9T_{cp}-\delta)^3} \\ &= 2\mathrm{e}^{-(2/3)D(\gamma G)^2(9T_{cp})^3}\mathrm{e}^{-DK^2 18T_{cp}} \\ &\quad \times \cosh\left\{2K^2D[(9T_{cp})^2/\delta + \delta/3]\right\}. \end{aligned} \tag{11}$$

The cosh factor for the above pathways may not be approximated by 1 and the contribution from this pathway can deviate from our ansatz in Eq. (7). However, coherence pathways such as $Q = (+++++-----)$ do not contribute much to the CPMG and KCPMG echoes, because with our pulse sequences, they are only ineffectively excited and they do not have large degeneracies. A detailed analysis of CPMG coherence pathways and their classification [11] has shown that the main contribution to the CPMG signals comes from two

classes of coherences, the direct echo and the so-called singly stimulated echoes. The term singly stimulated echo refers to those pathways with no consecutive + or − present. For these pathways, the spatial modulation of the phase is always characterized by wave vectors with a magnitude less than $\gamma G T_{cp}$. The basic segment of the singly stimulated coherence pathway is

$$-\underbrace{0\cdots0}_{s_1}+ \quad \text{and} \quad +\underbrace{0\cdots0}_{s_1}-, \tag{12}$$

where s_1 is the number of $q = 0$ in such segments. The direct echo can be seen as the special case with $s_1 = 0$. Contributions from these two classes account for about 95% of the CPMG signal. Furthermore, the average length of such segments has been found to be very short for CPMG, $s_1 \lesssim 2$. These results illustrate a fundamental characteristic of the coherence pathways in CPMG and related sequences, that the basic segments are the direct spin echo segments, $+-$, and short singly stimulated segments with s_1 being around 2. The CPMG signals should be attributed primarily to the pathways formed by these short segments as the repeating units.

Let us consider a singly stimulated segment, $+0\cdots0-$ with s_1 zeros. Using the Hahn's formula for stimulated echo attenuation [29], we calculate the decay component (summing both positive and negative T_m)

$$\begin{aligned} S_Q &= \mathrm{e}^{-D(\gamma G)^2(T_{cp}-\delta)^2(2T_{cp}-2\delta+6s_1T_{cp})/3} \\ &\quad + \mathrm{e}^{-D(\gamma G)^2(T_{cp}+\delta)^2(2T_{cp}+2\delta+6s_1T_{cp})/3} \\ &= 2\mathrm{e}^{-D(\gamma G)^2(2/3+2s_1)T_{cp}^3} \times \mathrm{e}^{-DK^2(2+2s_1)T_{cp}} \\ &\quad \times \cosh\left(D(\gamma G)^2((2+4s_1)T_{cp}^2\delta + 2\delta^3/3)\right). \end{aligned} \tag{13}$$

The first term, $\exp[-D(\gamma G)^2(2/3+2s_1)T_{cp}^3]$, is the same for the CPMG contribution. The second term $\exp[-DK^2(2+2s_1)T_{cp}]$ is the KCPMG factor. When s_1 is small and $D(\gamma G)^2T_{cp}^3$ is small, the cosh term approximates 1 to second order and thus this contribution is consistent with Eq. (7).

4.1. KCPMG to monitor other processes

We have shown that KCPMG is capable of monitoring molecular displacement as a function of echo time. It is natural to extend it to monitor coherent movement of molecules, such as in a flowing fluid. In particular, since this experiment measures displacement as a function of time, it should be able to obtain velocity and acceleration in a non-stationary flow.

In general, KCPMG is capable of monitoring evolution of magnetization and it may be useful to study other processes, for example, magnetization transfer via chemical exchange. This process is commonly measured by first perturbing the spin system out of equilibrium and then monitoring its evolution as a function of time, Δ. Usually, experiments have to be repeated for different Δ in order to characterize the dynamics over a range of time scales. Using KCPMG (in this case without field gradient), the entire Δ-dependence can be obtained in one or a few scans. For example, consider a two-proton system with a difference in resonant frequency f due to chemical shifts. Let $T_m = \pm 1/2f$, then the spins of the two protons will point to the opposite directions at the beginning of the CPMG portion of KCPMG [Eq. (3)]. Then, KCPMG echoes will reflect the evolution of the initial state with two opposite-pointing spins. The relative short acquisition window ($2T_{cp}$) will limit the spectral resolution.

4.2. Limitations

KCPMG echoes are only formed when

$$|T_m| < T_{cp}. \tag{14}$$

This limits the amount of phase encoding that can be achieved by the choice of the echo spacing in the CPMG sequence. This puts a restriction on the range of diffusion constant that can be measured using this technique for a given field gradient. If T_{cp} is increased too much, the total number of observable echoes becomes too small for signal-to-noise consideration. With a field gradient of 10 G/cm, it is difficult to measure diffusion constants much lower than 10^{-6} cm^2/s. Higher field gradients will be helpful to reduce T_{cp} and T_m and expand the detectable range of diffusion constants.

The uncertainties in the extracted value of the time-dependent diffusion coefficient from KCPMG depends on time. At early time, the diffusion effect is small, possibly resulting in large errors. At very long times, the relative attenuation is large, but the overall amplitudes are very small. This may lead again to large errors.

5. Conclusions

This paper presents a novel concept to extend the CPMG sequence to detect molecular displacement at many time points in one scan of the sequence. The essence of our modification to the CPMG sequence is to modulate the initial magnetization and then to observe the evolution of such modulation with the CPMG π pulse train. Despite the complexity of the coherence pathways in CPMG and KCPMG, we provide an intuitive understanding of the sequence. This new method enables a rapid measurement of diffusion in bulk fluids and most importantly in porous media where the diffusion process is restricted by the pore geometry. This method might be particularly useful for applications of hyperpolarized gases, such as xenon and helium, or other non-equilibrium magnetization sources where it is difficult to maintain a sufficiently stable supply for multiple experiments. Using the KCPMG concept, only

a few scans will be needed to obtain results for many diffusion times.

Acknowledgments

The authors thank P. Speier for pointing out the work of K.J. Packer and discussions with P.N. Sen on the theory of diffusion in porous media.

Appendix A. Theory

This section presents the theory of KCPMG for bulk diffusion by analyzing the contributing coherence pathways similar to those described for CPMG previously [11,21]. We will first review the coherence pathways for CPMG before investigating the coherence pathways for KCPMG. The theory is presented specifically for the pulse sequence in Eq. (3).

A.1. Coherence pathways for CPMG

We follow the notations used in [21] in defining three states of spin magnetization of an ensemble of spin-1/2 nuclei, M_0, M_-, and M_+:

$$\begin{aligned} M_0 &= M_z, \\ M_+ &= M_x + \mathrm{i}M_y, \\ M_- &= M_x - \mathrm{i}M_y. \end{aligned} \tag{A.1}$$

These states are marked by q which can be 0, +1, and −1, (or 0, +, and −) respectively. The RF pulses rotate the magnetization vector and thus change q,

$$\mathbf{M}(t_p) = \mathbf{R}\cdot\mathbf{M}(0). \tag{A.2}$$

Here, $\mathbf{M}(0)$ and $\mathbf{M}(t_p)$ are the magnetization vectors before and after the pulse and the pulse duration is t_p. $\mathbf{R}$ depends on the Larmor frequency offset from the RF frequency ω_{RF}, $\Delta\omega_0 \equiv \gamma|B_0| - \omega_{\mathrm{RF}}$, ω_1, and t_p. Then, the nutation frequency is $\Omega \equiv \sqrt{\omega_1^2 + \Delta\omega_0^2}$ where $\omega_1 = \gamma B_1/2$, and the tipping angle is Ωt_p. The matrix elements, $R_{l,m}$, are given in [21] and repeated here

$$\begin{aligned} R_{+,+} &= R^*_{-,-} \\ &= \frac{1}{2}\left\{\left(\frac{\omega_1}{\Omega}\right) + \left[1 + \left(\frac{\Delta\omega_0}{\Omega}\right)^2\right]\cos(\Omega t_p)\right\} \\ &\quad + \mathrm{i}\left(\frac{\Delta\omega_0}{\Omega}\right)\sin(\Omega t_p), \end{aligned} \tag{A.3}$$

$$R_{0,0} = \left(\frac{\Delta\omega_0}{\Omega}\right)^2 + \left(\frac{\omega_1}{\Omega}\right)^2\cos(\Omega t_p), \tag{A.4}$$

$$\begin{aligned} R_{+,0} &= R^*_{-,0} \\ &= \frac{\omega_1}{\Omega}\left\{\frac{\Delta\omega_0}{\Omega}[1-\cos(\Omega t_p)] - \mathrm{i}\,\sin(\Omega t_p)\right\}\mathrm{e}^{+\mathrm{i}\phi}, \end{aligned} \tag{A.5}$$

$$\begin{aligned} R_{0,+} &= R^*_{0,-} \\ &= \frac{\omega_1}{\Omega}\left\{\frac{\Delta\omega_0}{\Omega}[1-\cos(\Omega t_p)] - \mathrm{i}\,\sin(\Omega t_p)\right\}\mathrm{e}^{-\mathrm{i}\phi}, \end{aligned} \tag{A.6}$$

$$R_{+,-} = R^*_{-,+} = \frac{1}{2}\left(\frac{\omega_1}{\Omega}\right)^2[1-\cos(\Omega t_p)]\mathrm{e}^{+\mathrm{i}2\phi}. \tag{A.7}$$

In this paper, the rotations for the π/2 and π pulses are labelled as $L_{q,q'}$ and $\Lambda_{q,q'}$, respectively.

A coherence pathway is characterized by a series of numbers, $Q_N \equiv (q_0, q_1, \ldots, q_N)$, where q_0 is the magnetization state before the first π pulse and N is the echo number. Ref. [11] has presented a classification of the major coherence pathways showing the importance of two classes of coherences, the direct spin echo (SE) and the stimulated echo (STE).

In the absence of spin relaxation, the Nth echo signal is obtained from a sum over all coherence pathways ($M(N) = \sum_{Q_N} M_{Q_N}$) where each term can be written as a product of two factors

$$\begin{aligned} M_{Q_N} &= A_Q \cdot S_Q \\ &= \left(L_{0,q_0}\prod_{l=1}^{N}\Lambda_{q_l,q_{l-1}}\right)\left\langle \exp\left(\mathrm{i}\sum_{l=0}^{N} q_l\phi_l\right)\right\rangle. \end{aligned} \tag{A.8}$$

Here, $L_{qq'}$ and $\Lambda_{qq'}$ are matrix elements of the π/2 and π pulses and A_Q is identical for KCPMG and CPMG for the same coherence pathway. Also, A_Q depends on the frequency offset and the RF power. ϕ_l is the random phase factor due to diffusion between pulse l and $l+1$ in the presence of magnetic field gradients. The angle brackets $\langle\cdots\rangle$ represent an ensemble average of the random phase factors, $\phi_0, \phi_1, \phi_2, \ldots, \phi_N$. S_Q does not depend on frequency offset. For unrestricted diffusion, this contribution can be written as [21,30]

$$S_Q = \exp\left(-\frac{2}{3}\eta_{Q_N}\gamma^2G^2DT_{cp}^3N\right), \tag{A.9}$$

where η_{Q_N} is the enhancement of the decay rate for Q_N compared to that of the direct echo pathway. Also, G is the applied field gradient, D is the bulk diffusion constant, and T_{cp} the half of the time between adjacent π pulses.

A.2. Analytical results for early KCPMG echoes

For the echoes after the first and second π pulses, the coherences are limited to Hahn echoes and stimulated echoes. The diffusion effects for them have been calculated by Hahn [29].

Echoes after first π pulse

Only contribution from direct echo coherence, CPMG:

$$S_1 = \mathrm{e}^{-(2/3)D(\gamma G)^2T_{cp}^3}. \tag{A.10}$$

KCPMG (adding the signals for $T_m > 0$ and $T_m < 0$):

$$S_1 = e^{-(2/3)D(\gamma G)^2(T_m+T_{cp})^3} + e^{-(2/3)D(\gamma G)^2(T_m-T_{cp})^3}$$
$$= e^{-(2/3)\alpha-2D(\gamma G)^2T_m^2T_{cp}} \cdot \left[e^{-D(\gamma G)^2(T_{cp}^2T_m-T_m^3/3)} + e^{D(\gamma G)^2(T_{cp}^2T_m+T_m^3/3)}\right] \quad (A.11)$$
$$\approx e^{-(2/3)\alpha-2DK^2T_{cp}}\left[2+O(\alpha^2)\right]. \quad (A.12)$$

where $K = \gamma G T_m$, $\alpha = D(\gamma G)^2 T_{cp}^3$ and we assume $\alpha \ll 1$. $O(\alpha^2)$ denotes a term second order in α.

The coherence pathways in CPMG and KCPMG for these echoes are identical, thus the matrix elements (A_Q) determining the weight of these pathways are the same [21]. Hence, the ratio of the KCPMG data and the CPMG data is approximately $\exp[-K^2D \cdot 2T_{cp}]$.

Echoes after the second π pulse

CPMG:

$$\text{SE}: \quad e^{-(4/3)\alpha}, \quad (A.13)$$

$$\text{STE}: \quad e^{-(8/3)\alpha}. \quad (A.14)$$

KCPMG: $T_m < 0$:

$$\text{SE}: \quad e^{-(2/3)D(\gamma G)^2(T_{cp}-T_m)^3}e^{-(2/3)D(\gamma G)^2(T_{cp}+T_m)^3} = e^{-(4/3)\alpha-D(\gamma GT_m)^2 4T_{cp}}, \quad (A.15)$$

$$\text{STE}: \quad e^{-D(\gamma G)^2(T_{cp}-T_m)^2(8T_{cp}-2T_m)/3}. \quad (A.16)$$

KCPMG: $T_m > 0$:

$$\text{SE}: \quad e^{-(2/3)D(\gamma G)^2(T_{cp}+T_m)^3}e^{-(2/3)D(\gamma G)^2(T_{cp}-T_m)^3} = e^{-(4/3)\alpha-D(\gamma GT_m)^2 4T_{cp}} \quad (A.17)$$

$$\text{STE}: \quad e^{-D(\gamma G)^2(T_{cp}+T_m)^2(8T_{cp}+2T_m)/3}. \quad (A.18)$$

Combining signals from positive and negative T_m,

$$\text{SE}: \quad 2e^{-(4/3)\alpha-DK^2 4T_{cp}}, \quad (A.19)$$

$$\text{STE}: \quad e^{-(8/3)\alpha-DK^2 4T_{cp}}\left[2+O(\alpha^2)\right]. \quad (A.20)$$

The frequency spectra of these coherence pathways are determined by the matrix elements (A_Q) and have been shown in [21]. The amplitudes of the two coherence pathways depend on the RF pulses and the frequency filtering in detection. Let A_{SE} and A_{STE} denote these amplitudes, thus we can express the KCPMG signal as

$$M_2 \approx 2A_{SE}e^{-(4/3)\alpha-DK^2 4T_{cp}} + 2A_{STE}e^{-(8/3)\alpha-DK^2 4T_{cp}}$$
$$= e^{-DK^2 4T_{cp}} \times \left[2A_{SE}e^{-(4/3)\alpha} + 2A_{STE}e^{-(4/3)\alpha}\right]. \quad (A.21)$$

The factor between the square brackets is precisely the signal for the second CPMG echo.

A.3. KCPMG echoes after many π pulses

For the KCPMG sequence, for example, Eq. (3), the contribution from a coherence pathway Q is a product of two factors,

$$M_{Q_N} = A_Q \cdot S_Q^K. \quad (A.22)$$

A_Q is the product of the matrix elements associated with the RF pulses and is identical to the corresponding term for CPMG. The factor S_Q^K is the diffusion decay factor that include the initial magnetization modulation $\exp(\pm i\Delta\omega_0|T_m|)$. The S_Q^K factor is in general different from the corresponding term for CPMG.

In order to understand S_Q^K, it is useful to introduce for each coherence pathway the instantaneous wavevector $k(t)$ in analogy to the approach in magnetic resonance imaging:

$$k(t) = \gamma G \int_0^t q(t')\,dt', \quad (A.23)$$

where $q(t')$ is the instantaneous value of q that is piecewise constant between pulses. The diffusive attenuation for a given coherence pathway and unrestricted diffusion can then generally be written as [3]

$$S_Q^K = \exp\left\{-D\int_0^T k(t)^2\,dt\right\}, \quad (A.24)$$

where time $t = 0$ is defined at the beginning of the sequence Eq. (3) and T is the echo time. The inclusion of T_m in the initial pulse spacing of the KCPMG sequence leads to a shift of the instantaneous wavevector of K relative to that in the CPMG sequence. We use $k(t)$ to denote the instantaneous wavevector for the CPMG sequence. Up to corrections of order $\exp(D\gamma^2G^2\delta^3)$, the diffusive attenuation can be written as:

$$S_Q^K(K,t) \approx \exp\left\{-D\int_{T_m}^{T_m+2NT_{cp}}[k(t)+K]^2\,dt\right\}$$
$$= S_Q(2NT_{cp}) \times \exp\left\{-DK^2 \cdot 2NT_{cp}\right\} \times \exp\left\{-2DK\int_{T_m}^{2NT_{cp}} k(t)\,dt\right\}. \quad (A.25)$$

The integral limits T_m and $T_m + 2NT_{cp}$ correspond to the beginning and the echo position of the CPMG sequence. This factorization thus facilitates comparison with the CPMG sequence, for instance, $S_Q(2NT_{cp})$ is the decay factor for CPMG. This expression shows that for symmetrical coherence pathways such as the direct echo, $\int_0^t k(t)\,dt = 0$ and the last term can be replaced by 1. In this case, our ansatz for the KCPMG sequence is recovered. However, for a general coherence pathway, the last term is not exactly 1 and the ansatz becomes an approximation. The key question is whether the signal is dominated by contributions from coherence pathways where the correction term is small or not. Our experimental results indicate that the ansatz is indeed a good approximation. We find further support in numerical calculations, where we calculated the weight and diffusive attenuation for all coherence pathways that contribute signal up to the 15th echoes. Similar to our

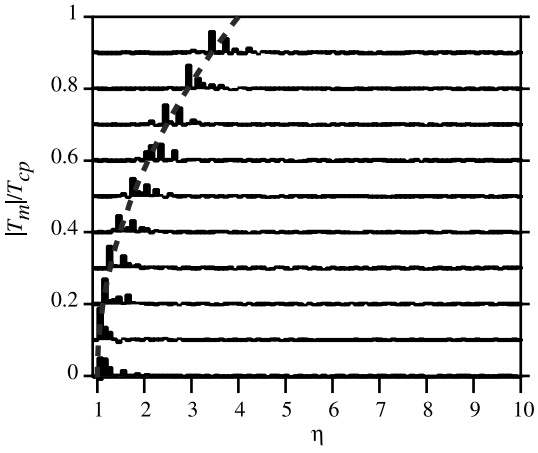

Fig. 7. Calculated diffusion decay factor η for the coherence pathways of the 15th echo, as $|T_m|/T_{cp}$ increases. The enhancement of η as $|T_m|/T_{cp}$ increases is consistent with the behavior of Eq. (7), as indicated by the dashed line.

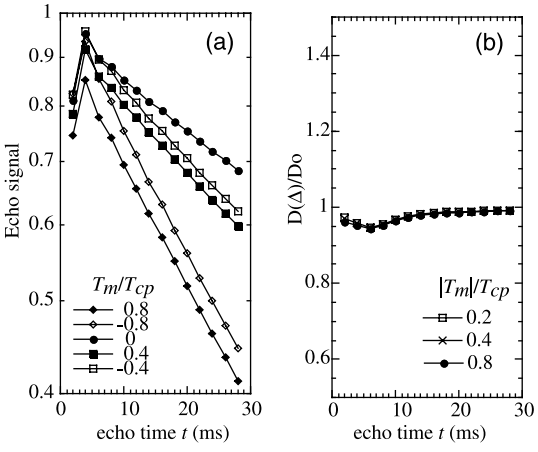

Fig. 8. (a) Calculated KCPMG echo amplitudes of the first 14 echoes, for $T_m/T_{cp} = \pm 0.8, \pm 0.4$, and 0. (b) Time-dependent diffusion constant calculated from above KCPMG echoes using Eq. (7). The parameters used are: $G = 40$ G/cm, $T_{cp} = 1$ ms, and $D = 2.3 \times 10^{-5}$ cm^2/s.

treatment of CPMG echoes, we parametrize the diffusion factor S_Q^K as

$$S_Q^K = \exp\left(-\frac{2}{3}\eta_{Q_N}\gamma^2 G^2 D T_{cp}^3 N\right). \quad \text{(A.26)}$$

The numerical results are summarized below.

Fig. 7 shows the diffusion decay factor η for the coherence pathways of the 15th echo, summing the contribution from positive and negative T_m. As $|T_m|/T_{cp}$ increases, the diffusion rate for the major coherence pathways increases and the increase is approximately proportional to K^2, consistent with Eq. (7). We have further calculated the KCPMG echoes by summing all coherence pathways, then obtained the signal intensity using a filter that is of the shape of asymptotic CPMG echo shifted to the corresponding KCPMG echo positions. These echo amplitudes are used to calculate $D(t)$ by Eq. (7), and the results are shown in Fig. 8.

References

[1] D.E. Woessner, NMR spin-echo self-diffusion measurements on fluids undergoing restricted diffusion, J. Phys. Chem. 67 (1963) 1365.
[2] P.P. Mitra, P.N. Sen, L.M. Schwartz, P. Le Doussal, Diffusion propagator as a probe of the structure of porous media, Phys. Rev. Lett. 24 (1992) 3555.
[3] E.O. Stejskal, J.E. Tanner, Spin diffusion measurements: spin echoes in the presence of a time-dependent field gradient, J. Chem. Phys. 42 (1965) 288.
[4] J.E. Tanner, E.O. Stejskal, Restricted self-diffusion of protons in colloidal systems by the pulsed-gradient, spin-echo method, J. Chem. Phys. 49 (1968) 1768.
[5] M.D. Hürlimann, L. Venkataramanan, Quantitative measurement of two-dimensional distribution functions of diffusion and relaxation in grossly inhomogeneous fields, J. Magn. Reson. 157 (2002) 31.
[6] H.Y. Carr, E.M. Purcell, Effects of diffusion on free precession in NMR experiments, Phys. Rev. 94 (1954) 630.
[7] S. Meiboom, D. Gill, compensation for pulse imperfections in Carr–Purcell NMR experiments, Rev. Sci. Instrum. 29 (1958) 688.
[8] T.M. de Swiet, P.N. Sen, Decay of nuclear magnetization by bounded diffusion in a constant field gradient, J. Chem. Phys. 100 (1994) 5597.
[9] P.N. Sen, A. Andre, S. Axelrod, Spin echoes of nuclear magnetization diffusing in a constant magnetic field gradient and in a restricted geometry, J. Chem. Phys. 111 (1999) 6548.
[10] L.J. Zielinski, P.N. Sen, Relaxation of nuclear magnetization in a nonuniform magnetic field gradient and in a restricted geometry, J. Magn. Reson. 147 (2000) 95.
[11] Y.-Q. Song, Categories of coherence pathways in the CPMG sequence, J. Magn. Reson. 157 (2002) 82.
[12] K.J. Packer, The study of slow coherent molecular motion by pulsed nuclear magnetic resonance, Mol. Phys. 17 (1969) 355.
[13] M.D. Hürlimann, Optimization of timing in the Carr–Purcell–Meiboom–Gill sequence, Magn. Reson. Imaging 19 (2001) 375.
[14] R. Kaiser, E. Bartholdi, R.R. Ernst, Diffusion and field-gradient effects in NMR Fourier spectroscopy, J. Chem. Phys. 60 (1974) 2966.
[15] A.L. Bloom, Nuclear induction in inhomogeneous fields, Phys. Rev. 98 (1955) 1105.
[16] J. Hennig, Multiecho imaging sequences with low refocusing flip angles, J. Magn. Reson. 78 (1988) 397.
[17] G. Goelman, M.G. Prammer, The CPMG pulse sequence in strong magnetic field gradients with applications to oil-well logging, J. Magn. Reson. A 113 (1995) 11.
[18] J. Simbrunner, R. Stollberger, Analysis of Carr–Purcell sequences with nonideal pulses, J. Magn. Reson. B 109 (1995) 301.
[19] A. Ross, M. Czisch, G.C. King, Systematic errors associated with CPMG pulse sequence and their effect on motional analysis of biomolecules, J. Magn. Reson. 124 (1997) 355.
[20] F. Bălibanu, K. Hailu, R. Eymael, D.E. Demco, B. Blümich, Nuclear magnetic resonance in inhomogeneous magnetic field, J. Magn. Reson. 145 (2000) 246.
[21] M.D. Hürlimann, Diffusion and relaxation effects in general stray field NMR experiments, J. Magn. Reson. 148 (2001) 367.
[22] K. Oshio, F.A. Jolesz, Fast MRI by creating multiple spin echoes in a CPMG sequence, Magn. Reson. Med. 30 (1993) 251.

[23] P.T. Callaghan, Principles of Nuclear Magnetic Resonance Microscopy, Oxford University Press, New York, 1993.
[24] A. Sodickson, D.G. Cory, A generalized k-space formalism for treating the spatial aspects of a variety of NMR experiments, Prog. NMR Spectrosc. 33 (1998) 77.
[25] P.N. Sen, L.M. Schwartz, P.P. Mitra, B.I. Halperin, Surface relaxation and the long-time diffusion coefficient in porous media: periodic geometries, Phys. Rev. B 49 (1994) 215.
[26] C. Straley, private communication, 2001.
[27] R.C. Wayne, R.M. Cotts, Nuclear-magnetic-resonance study of self-diffusion in a bounded medium, Phys. Rev. 151 (1966) 264.
[28] M.D. Hürlimann, K.G. Helmer, C.H. Sotak, Dephasing of Hahn echo in rocks by diffusion in susceptibility-induced field inhomogeneities, Magn. Reson. Imaging 16 (1998) 535.
[29] E.L. Hahn, Spin echoes, Phys. Rev. 80 (1950) 580.
[30] D.E. Woessner, Effects of diffusion in nuclear magnetic resonance spin-echo experiments, J. Chem. Phys. 34 (1961) 2057.